

Flipper-driven terrestrial locomotion of a sea turtle-inspired robot

Nicole Mazouchova¹, Paul B Umbanhowar² and Daniel I Goldman³

¹ School of Biology, Georgia Institute of Technology, Atlanta, GA, USA

² Department of Mechanical Engineering, Northwestern University, Evanston, IL, USA

³ School of Physics, Georgia Institute of Technology, Atlanta, GA, USA

E-mail: daniel.goldman@physics.gatech.edu

Received 19 November 2012


Accepted for publication 26 March 2013

Published 23 April 2013

Online at stacks.iop.org/BB/8/026007

Abstract

To discover principles of flipper-based terrestrial locomotion we study the mechanics of a hatchling sea turtle-inspired robot, FlipperBot (FBot), during quasi-static movement on granular media. FBot implements a symmetric gait using two servo-motor-driven front limbs with flat-plate flippers and either freely rotating or fixed wrist joints. For a range of gaits, FBot moves with a constant step length. However, for gaits with sufficiently shallow flipper penetration or sufficiently large stroke, per step displacement decreases with each successive step resulting in failure (zero forward displacement) within a few steps. For the fixed wrist, failure occurs when FBot interacts with ground disturbed during previous steps, and measurements reveal that flipper generated forces decrease as per step displacement decreases. The biologically inspired free wrist is less prone to failure, but slip-induced failure can still occur if FBot pitches forward and drives its leading edge into the substrate. In the constant step length regime, kinematic and force-based models accurately predict FBot's motion for free and fixed wrist configurations, respectively. When combined with independent force measurements, models and experiments provide insight into how disturbed ground leads to locomotory failure and help explain differences in hatchling sea turtle performance.

 Online supplementary data available from stacks.iop.org/BB/8/026007/mmedia

(Some figures may appear in colour only in the online journal)

1. Introduction

Animals swim, walk, run or burrow in a diversity of environments [1, 5] and with adeptness unmatched by the best human-made devices. While much progress has been made understanding aerial and aquatic locomotion [23], far less is known of the mechanisms by which organisms like lizards, crabs, turtles and cockroaches move with agility and stability over complex terrestrial ground like stones, leaf litter and sand [6]. Of interest to us are substrates that yield upon foot or body interaction, especially granular media, e.g. the sand found in deserts and beach environments [11]. Many organisms crawl and walk effectively on sand, some with remarkable performance [13, 17].

Granular substrates differ from fluids in that they remain solid until an applied load exceeds the yield stress at which

point the substrates flow in the vicinity of the load [17]. However, unlike true fluids, intrusion forces in granular substrates [28] are insensitive to rate for speeds less than $\sim 10 \text{ cm s}^{-1}$ [24] and exhibit hysteresis. Further, these substrates 'recall' previous disturbances. Because of these features, fundamental theory to describe limb-ground interaction is not yet available. Granular substrates are of practical importance since legged robots (like the cockroach-inspired hexapedal robot RHex [20]) can, in general, locomote successfully over hard ground or uneven complex terrain, e.g. forest floor [3], while their mobility can be limited on yielding substrates such as rubble or sand [15]. The lack of a fundamental theory for yielding ground has prevented the rational design of feet, limbs and controllers for robots that locomote on these substrates.

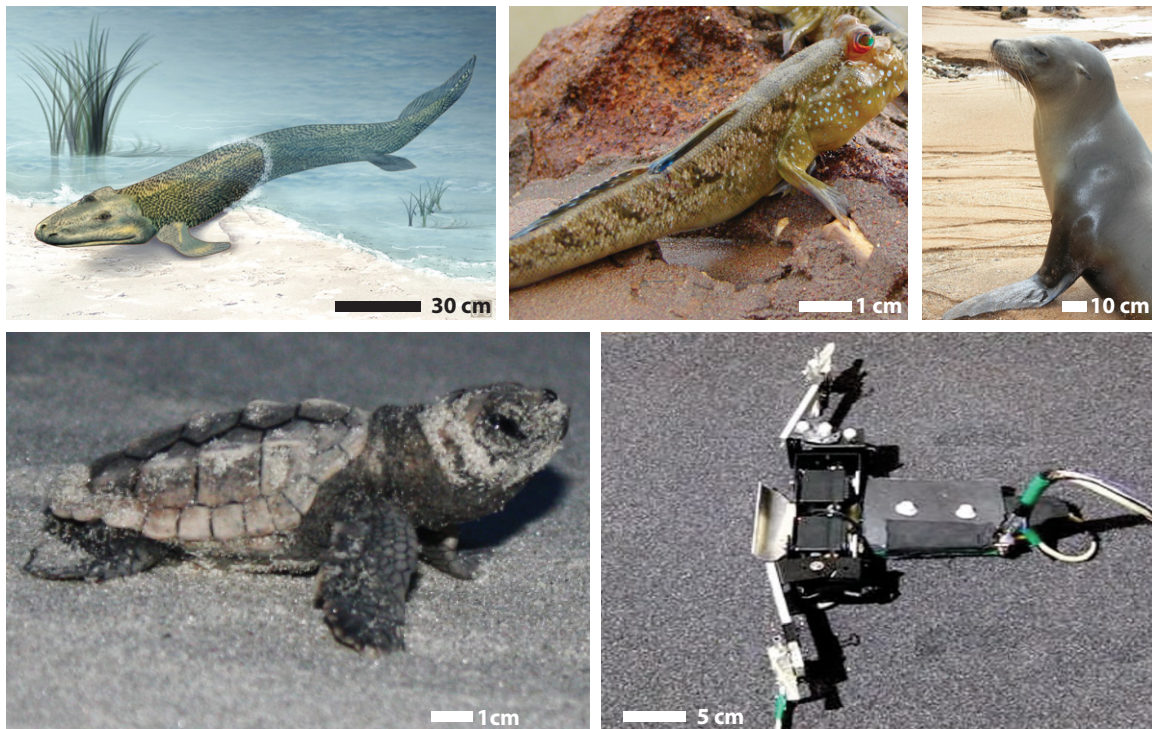


Figure 1. Locomotion using flippers or fins. Top: early tetrapod walkers such as *Tiktaalik* (image courtesy of Zina Deretsky, NSF) or modern aquatically adapted animals (mudskipper or sea lion; images courtesy of Bjorn ChristianTorrissen and flickr.com: sly06) use fins and flippers to traverse sandy terrestrial environments. Bottom-left: hatchling loggerhead sea turtle. Bottom-right: FBot, a sea turtle-inspired physical model.

A number of animals (e.g. seals, mudskippers and sea turtles, see figure 1) propel themselves on terrestrial granular substrates using appendages that are morphologically adapted for generating thrust and lift in aquatic environments [7, 22]. For example, adult sea turtles [26], which are effective ocean swimmers, often crawl hundreds of meters over sandy beaches to and from nesting areas [9], while their young, after incubation and hatching, dig themselves out of the nest and dash up to thousands of body lengths over yielding sand to the ocean. Early transitional forms like *Tiktaalik* [2, 27] are also thought to have propelled themselves on soft materials using fin-like appendages (figure 1) [29–31].

Research on how animals with aquatically adapted appendages, such as flippers, traverse granular terrestrial environments is in its infancy [26]. In our previous study of the locomotion of loggerhead sea turtle hatchlings (*Caretta caretta*) [17], we discovered that on hard ground the turtles propelled themselves forward by pivoting their limb about substrate asperities engaged with a claw (nail) while maintaining a rigid wrist. In contrast, on soft sand, we found that the turtle's large thin front flipper intruded into the granular medium at each step, and then bent at the wrist during forward locomotion [17]. When limbs did not slip during stance, soft sand performance of the turtles was comparable to that on hard ground. We hypothesized that the limb bending enhanced substrate solidification allowing the animals to achieve higher performance.

Discovery of principles by which flippers propel turtles on land using animal studies alone is challenging because

systematically manipulating animal gaits and morphology is impossible in most cases and because controlling the environment and maintaining access to study subjects is often difficult in field studies. Physical models, i.e. robots, allow the investigation of a particular aspect of morphology or control while interacting with a real world environment. Studying physical models can generate quantitative biological hypotheses [12]. For example, we previously studied SandBot (derived from the RHex series of cockroach-inspired robots [20]), and discovered that legged locomotion was sensitive to changes in limb kinematics and granular media compaction [15]. Top speeds of $\sim 50\%$ of SandBot's hard ground speed were achieved when limb kinematics were adjusted to minimize ground yield [14] and each step advanced the robot sufficiently far from the material disturbed by previous footsteps. We hypothesized that organisms that crawl on sand could utilize these principles, and drag experiments in our previous turtle study supported this hypothesis. However, while tantalizing, the applicability of the results from the SandBot work are unclear, since the limb–ground interaction (rotary walking) differed from that of the sea turtle.

In this paper we gain insights into the mechanics responsible for the surprising granular locomotor capabilities of the hatchling sea turtles. To do so, we perform a detailed locomotion study of a sea turtle-inspired robot, FlipperBot (FBot), that uses flippers to move on a model granular substrate, see figure 1. Our study reveals important features of terrestrial flipper-based locomotion, answers questions raised by our previous hatchling sea turtle study [17] and

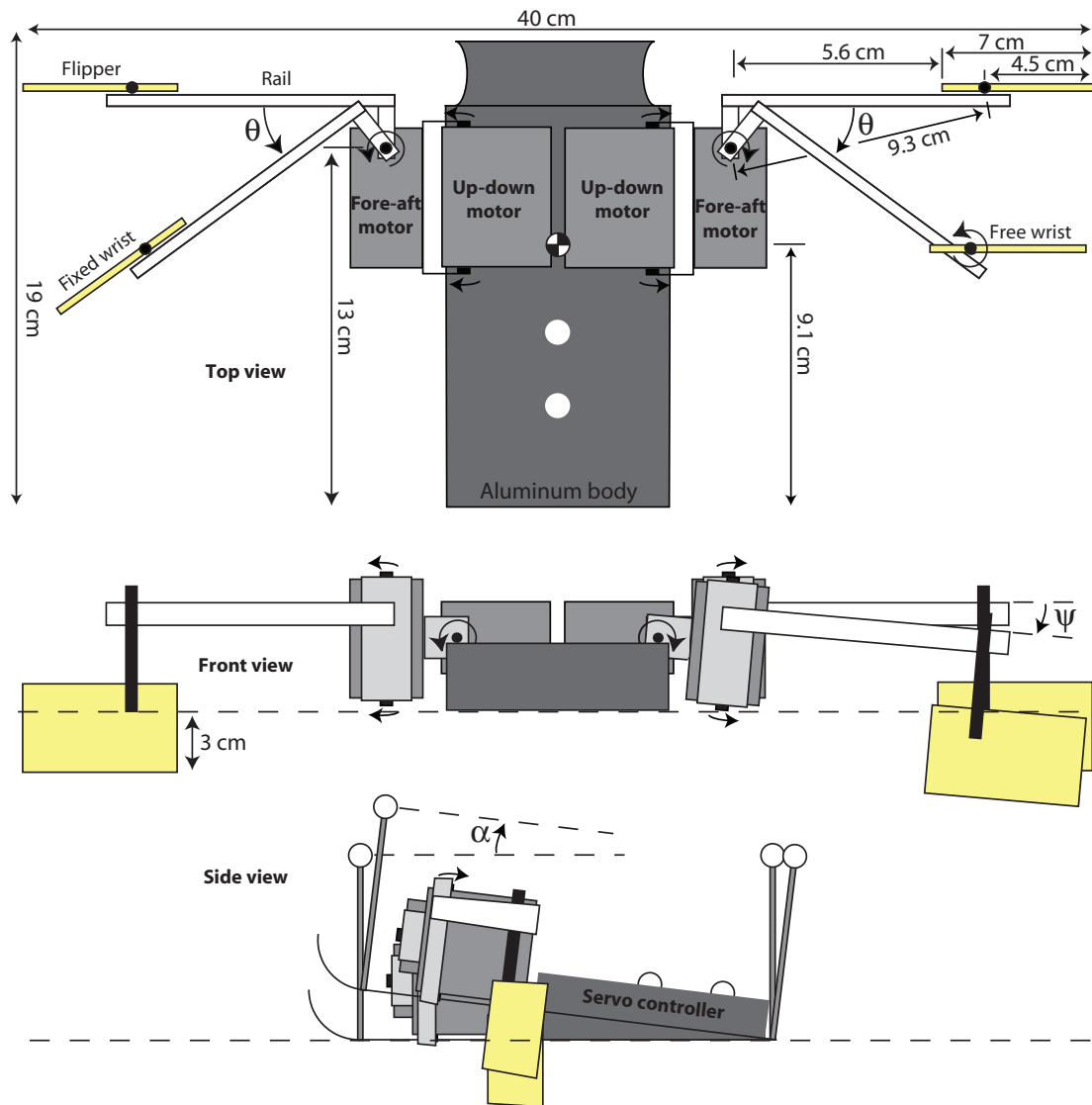


Figure 2. Drawings of FBot depicting stroke displacement θ , flipper insertion angle ψ and tilt angle α along with locations of flippers, servo-motors, markers for video tracking and COM (not to scale). Top-view contrasts flipper kinematics of freely rotating wrist (right wrist) to fixed wrist (left wrist).

introduces a new mode of robot locomotion. Section 2 describes the robot and experimental protocols. In section 3, we characterize the performance of different gaits and two wrist joint configurations, one fixed and one freely rotating that is inspired by the bent wrist employed by hatchling loggerhead sea turtles during sand locomotion [17]. We find that the free wrist outperforms the fixed wrist for nearly all gaits; however, failure occurs for both configurations when flippers interact sufficiently with ground disturbed during previous steps. We also observe similar disturbed ground associated decreases in locomotor performance in loggerhead sea turtle hatchlings. In section 4, we describe simple models to predict FBot's motion and compare their predictions to experiment. The models give insights into the mechanics of locomotory failure on yielding substrates. Section 5 discusses the relevance of our work to other flippered locomotors and summarizes our findings.

2. Materials and methods

2.1. FBot

FBot is a two-limbed, sea turtle-inspired locomotor with a 40 cm limb span and a mass of $m = 0.79$ kg, see figure 1. Its plastron-inspired base is a 19 cm \times 9 cm aluminum plate curved upward at the anterior and lateral edges. FBot's limbs are symmetric about the midline and attach near the anterior at a position comparable to the pectoral flippers of a sea turtle, see figure 2. Each limb connects to the base through a 'shoulder/elbow'-linkage formed by two servomotors (HiTec 5980SG). Each up-down shoulder motor is fixed to the base with its rotation axis parallel to the anteroposterior line. The fore-aft shoulder motor is connected to the up-down motor by a bracket such that the rotation axis of the fore-aft motor is perpendicular to the rotation axis of the up-down motor.

Each limb is attached to the fore–aft motor by a bracket such that it is orthogonal to the fore–aft motor’s rotation axis. The angular position of each up–down motor, ψ , was defined to be zero when the rotation axis of the fore–aft motor was vertical (limb horizontal); increasing ψ moved the limb downward. The angular position of each fore–aft motor, θ , was defined to be zero when the limb was perpendicular to the anteroposterior line; positive rotation from $\theta = 0$ moved the distal end of the limb toward the posterior.

Each lightweight limb consisted of a 11 cm \times 1.7 cm extruded aluminum rail with a distal, balsa wood flipper that extended 3 cm below the base when the rail was parallel with the plane of the base ($\psi = 0$). The 7 cm \times 4 cm \times 0.3 cm flipper was connected to the rail by a ‘wrist’ consisting of a 0.4 cm diameter, hollow, aluminum rod mounted on the flipper (which also minimized flipper flexing) and inserted in a plexiglass, plain bearing connected to the rail. The wrist axis was nominally vertical during the stance phase and was positioned 2.5 cm from the proximal end of the limb (9.3 cm from the fore–aft motor axis). The flipper had two distinct modes: free wrist and fixed wrist. In the free wrist mode (figure 2, top view, right side), the flipper, initially parallel to the rail, passively rotated during the ground contact. After the ground contact ended, the initial configuration was restored by a weak torsional spring (elastic band) attached to the wrist joint which rotated the flipper to a return stop on the rail but did not exert significant torques on the flipper during the ground contact. In the fixed wrist mode (figure 2, top view, left side), the flipper was held parallel to the rail by clamping it to the return stop, which prevented it from rotating relative to the rail.

2.2. Gait

A posterior mounted servo control board (Lynxmotion SSC-32) driven by a Python program controlled the limb kinematics (gait) via the four servomotors. The gait was symmetric and consisted of four stages. At the start of the first stage the limbs were orthogonal to the anteroposterior line ($\theta = 0$) at an angle of 45° above the surface ($\psi = -45^\circ$). In the first stage (‘insertion’) the up–down motors rotated the limbs downward until the flippers penetrated the ground. We used gaits with maximum insertion angles $-1.5^\circ < \psi_f < 1^\circ$, which corresponded to maximum potential insertion depths from 2.79 to 3.14 cm. In the second stage, or ‘step’ stage, the fore–aft motors rotated the limbs toward the posterior with final angles of $\theta_f = 45^\circ, 67^\circ$ and 90° . During the third stage, which ended the stance phase and began the swing phase, the flippers were removed from the ground by the up–down motors ($\psi \rightarrow -45^\circ$). In the fourth stage, the limbs were rotated forward by the fore–aft motors ($\theta \rightarrow 0$). The angular speed for all motors during the ground interaction was $\omega = 30^\circ \text{ s}^{-1}$, which gave a maximum flipper speed relative to FBot’s center of mass (COM) of $\approx 4 \text{ cm s}^{-1}$. We note that for the low relative ground speeds of the flippers used in our study, granular drag forces acting on the flippers were speed insensitive [24], i.e. dominated by the frictional force [32] as opposed to momentum transfer to the flowing ground.

2.3. Tracking and locomotion testing

A high-speed digital video camera (AVT Pike F-032) controlled by a LabView (NI LabView 2009) program with integrated tracking recorded side or top views of the locomotion. Two 16 cm long masts topped with light emitting diodes and mounted near the front and rear were used for side-view tracking, while two 1 cm diameter white plastic spheres attached to the servo control board cover were used for top-view tracking, see figure 2. All tracking markers were located along the anteroposterior axis. Position versus time data from the video tracking were analyzed using Matlab (MathWorks 2009).

FBot was tested on a 122 cm long, 60 cm wide and 10 cm deep bed of poppy seeds⁴ (mean diameter ~ 0.1 cm). The bed surface was leveled with a float before each run (resulting in a solids volume fraction of ≈ 0.62) after which FBot was carefully placed onto the surface with its flippers raised. During a run, FBot’s power and communication cable were positioned behind it and supported by a researcher to minimize extraneous forces and torques on the robot.

2.4. Controlled translation

To investigate the effect of ground disturbed by previous steps on the performance of FBot, we conducted a separate set of translation experiments in which FBot was placed on an undisturbed bed and executed a single step. After the initial step was complete, FBot was picked up and placed a distance Δd from its position prior to the first step ($1 \text{ cm} \leq \Delta d \leq 20 \text{ cm}$). FBot then executed a second step and the distance advanced during the second step was recorded. Note that when Δd was less than the displacement of the first step, FBot was moved backward relative to its position after the first step.

2.5. Lift and thrust

To characterize the forces generated by the flippers during the stance phase of the gait and their dependence on the distance from the previous step, separate force measurements were performed with a 2-axis, stepper motor-driven, linear translation stage configured to move vertically and horizontally. A flipper analogue made from a stainless steel plate⁵ (width 5 cm, height 22.5 cm, thickness 0.3 cm) was rigidly connected to a 6-axis force sensor (ATI Delta) attached to the translation stage. The poppy seed bed was prepared as in the FBot experiments. The force sensor recorded the vertical penetration force, F_p , as the flipper was pushed 3 cm into the substrate and the horizontal drag force, F_d , as the flipper was displaced 3 cm horizontally backward through the bed. At the end of the drag, the flipper was retracted from the bed and moved forward a distance Δd in advance of the first penetration, and the penetration and drag repeated. The speed of all movements was 0.5 cm s^{-1} . The force signals were captured with LabView and analyzed using Matlab.

⁴ The forces on intruders in poppy seeds and natural sand are similar, see [16].

⁵ There are no significant differences between the penetration and drag forces on intruders made of balsa wood and stainless steel as these forces are insensitive to the particle–intruder friction coefficient [21].

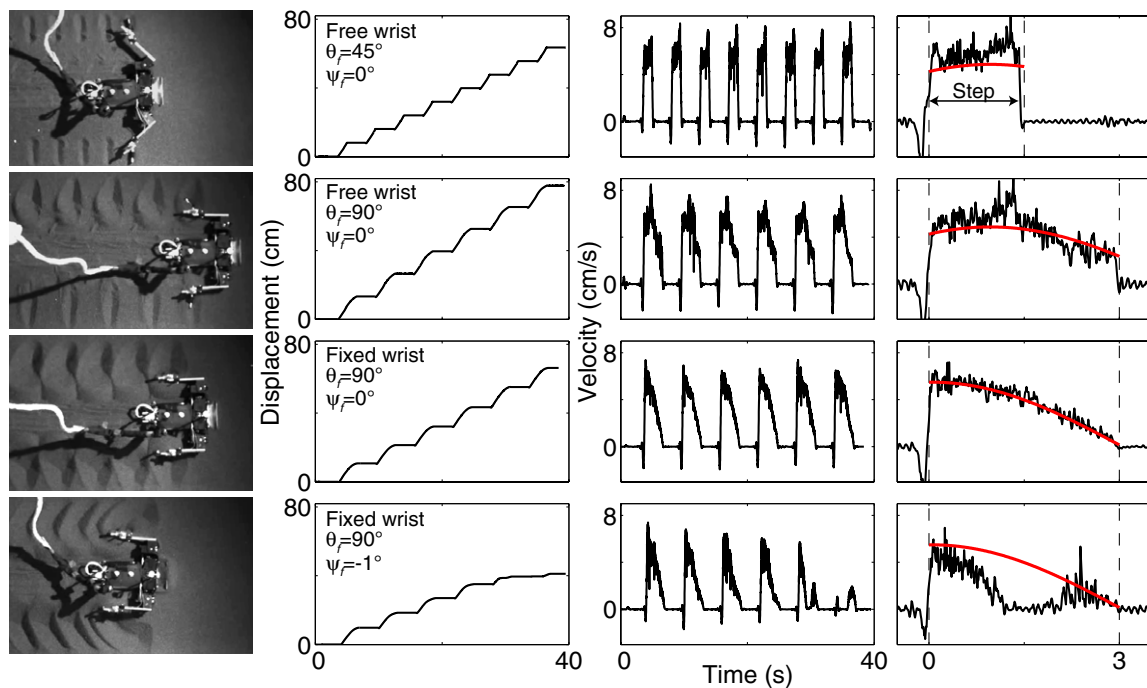


Figure 3. Kinematics of FBot comparing (rows 1–3) constant per step displacement gaits to (row 4) a gait exhibiting locomotory failure for various wrist configurations, stroke amplitudes, θ_f , and flipper insertion depths quantified by angle, ψ_f . Column 1: images after four steps from the same starting position showing differences in the total displacement and ground disturbance. Columns 2 and 3: displacement and velocity versus time. Column 4: single-step velocity versus time for fifth step (origin of time axis shifted to the start of fifth step). Red curves during step phase are from models of FBot locomotion, see section 4.

2.6. Sea turtle testing

Field work with loggerhead sea turtle hatchlings was conducted over a single six week period in 2010 on Jekyll Island, GA in collaboration with the Georgia Sea Turtle Center⁶. Two to five hatchlings were randomly selected from each of ten nests for a total of 25 animals. Hatchlings were transported from the nest in a sand-filled Styrofoam container to a fluidized bed trackway filled with Jekyll Island beach sand as in our previous study [17]. Two high speed IR cameras (Sony Handycam HDR-HC3 and HDR-HC5) recorded the motion of the hatchlings at 250 fps as they ran on loose (solids volume fraction ≈ 0.58) level media (66 runs). Only straight runs with near constant average velocity over a distance of at least 20 cm were accepted. Small, white removable markers attached to the carapace of the animals were used for tracking (top and side view). Kinematic data from the video tracking were analyzed using Matlab.

3. Results

3.1. Robot kinematics

FBot advanced in a start–stop motion with a near constant per step displacement (see, for example, the constant spacing between flipper tracks shown in the top three images of the first column of figure 3) for a wide range of stroke amplitudes, θ_f , and a smaller range of insertion depths

(characterized by ψ_f). Tracking data indicated that forward displacement occurred only during the step phase of the gait. For both free and fixed wrist configurations, FBot's per step displacement, ΔS , increased with increasing stroke amplitude θ_f at $\psi_f = 0$. For the same θ_f and ψ_f in the constant step displacement regime, FBot's average speed was nearly independent of the wrist configuration despite differences in the flipper–ground interaction. For the sea turtle-inspired free wrist, as the flippers were drawn backward the plane of each flipper remained in essentially the same orientation (perpendicular to the anteroposterior axis) as the body was propelled forward. During the stroke, flippers slid away and then toward the body but slipped little, if at all, in the fore–aft direction. In contrast, for the fixed wrist the flippers were constrained to rotate relative to the substrate during the stroke and, consequently, continuously yielded the material while simultaneously advancing the body.

Velocity profiles for the constant per step displacement gait parameters show that during the step stage the body was rapidly accelerated to a peak velocity and then decelerated to rest at each step for each wrist configuration. The duration of the step was equal to the duration of the fore–aft motor motion for both wrist configurations, indicating that the system was strongly overdamped and that inertia was unimportant for FBot at the chosen limb velocity ($\omega = 30^\circ \text{ s}^{-1}$). However, the shape of the velocity profile varied with the wrist configuration. For the free wrist, velocity peaked at $\theta \approx 40^\circ$ and then declined gradually with further increase in θ , see rows 1 and 2 of figure 3. For the fixed wrist, velocity was maximum at or near

⁶ State of Georgia Scientific Collecting Permit 29-WBH-10-108 and IACUC Permit A10005.

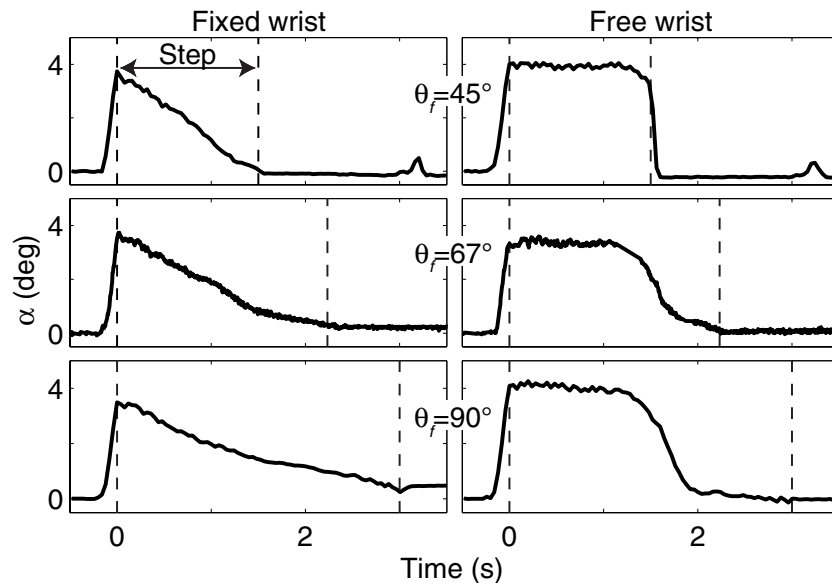


Figure 4. Tilt angle, α , versus time, t , for distinct gait amplitudes, θ_f , (rows) and wrist configurations (columns) for six non-failing gaits with $\psi_f = 0$. For the fixed wrist (left), α decrease continuously during the step with a rate that decreases with increasing θ_f . For the free wrist (right), α is nearly constant until it drops rapidly near $t = 1.7$ s ($\theta = 50^\circ$), as the COM moves ahead of the flippers. In all cases, maximum tilt is $\approx 4^\circ$ and occurs at the beginning of the step (end of insertion). Dashed vertical lines at $t = 0$ and $t = \theta_f/\omega$ mark the beginning and end of the step, respectively.

the beginning of the step and continuously decreased during the step, see row 3 of figure 3.

Each velocity profile shown in figure 3 for steady pace gait parameters exhibited a brief interval of negative velocity at the beginning of the step. This feature was associated with the upward tilt of the front of FBot which moved the tracking markers backward as the up-down motors drove the flippers into the bed and which occurred for sufficiently large ψ_f . A tracked side-view profile of FBot during stance allowed direct measurement of the tilt angle α . Figure 4 shows that, for $\psi_f = 0$, the same maximum lift of approximately $\alpha = 4^\circ$ occurred at the end of flipper insertion (beginning of step stage) independent of the wrist configuration, but that the evolution of α during the step depended strongly on the wrist configuration. For the fixed wrist, α immediately started to decrease when the flippers were drawn backward and reached zero near $\theta = 40^\circ$. The slope of α was smaller for larger θ_f . For the free wrist, α remained nearly constant for θ less than $\approx 40^\circ$ and then decreased rapidly to zero independent of θ_f .

The results discussed thus far are for gait parameters that produced constant per step displacement. However, not all combinations of gait parameters θ_f and ψ_f and wrist configuration produced motion with constant step size. For sufficiently shallow flipper penetration (small or negative ψ_f) or for larger stroke amplitude at fixed ψ_f in both wrist configurations, the per step displacement, ΔS , decreased with each successive step until FBot stopped advancing, a condition we refer to as ‘failure’, see for example row 4 of figure 3.

To determine the dependence of failure on the flipper insertion depth, we performed experiments at $\theta_f = 90^\circ$ that measured the step displacement on successive steps for $-1.5^\circ \leq \psi_f \leq 1^\circ$, which correspond to maximum potential flipper substrate insertion depths (i.e. $\alpha = 0$) between 2.79 cm and 3.14 cm, respectively. Figure 5 shows that

FBot maintained a constant step displacement for $\psi_f \geq 0$ with fixed wrists and for $\psi_f \geq -0.75^\circ$ with free wrists. Failure occurred, as evidenced by decreasing ΔS on successive steps, for $\psi_f \leq -0.5^\circ$ with fixed wrists and a shallower $\psi_f \leq -1^\circ$ with free wrists. For gaits that failed, successive step displacements decreased more rapidly as ψ_f was reduced, and at the shallowest insertion ($\psi_f = -1.5^\circ$), forward displacement occurred only on the first step. With the exception of $\psi_f = -1.5^\circ$, ΔS for the first step with the free wrist was nearly independent of ψ_f (and thus independent of whether the gait lead to failure); in contrast, ΔS for the first step was significantly reduced for the failure gaits of the fixed wrist ($\psi_f \leq -0.5^\circ$).

3.2. Disturbed ground

For steady pace gaits, flipper tracks (defined as regions of visibly disturbed ground) did not significantly overlap (see figure 6 and top three panels of the first column in figure 3), while all gaits that failed showed increasing track overlap as ΔS decreased, see the bottom-left panel of figure 3. To isolate the effects of ground disturbed by previous steps, we conducted experiments in which FBot took one step in an undisturbed bed and was then picked up and moved forward a distance $\Delta d - \Delta S_1$, where ΔS_n denotes the size of step n . After being moved, FBot executed a second step whose size, ΔS_2 , is plotted versus Δd in figure 7 for $\theta_f \in \{45^\circ, 67^\circ, 90^\circ\}$ and $\psi_f \in \{0, -1^\circ\}$ and for both wrist configurations. At sufficiently large Δd , $\Delta S_2 = \Delta S_1$ indicating that ground disturbed by the first step did not affect the second (closed symbols). However, below a critical distance, Δd_c , that depended on the gait and wrist configuration, $\Delta S_2 < \Delta S_1$ and ΔS_2 decreased with decreasing Δd (open symbols). Overall, gaits with larger stroke (θ_f), less downward flipper rotation (smaller ψ_f) or

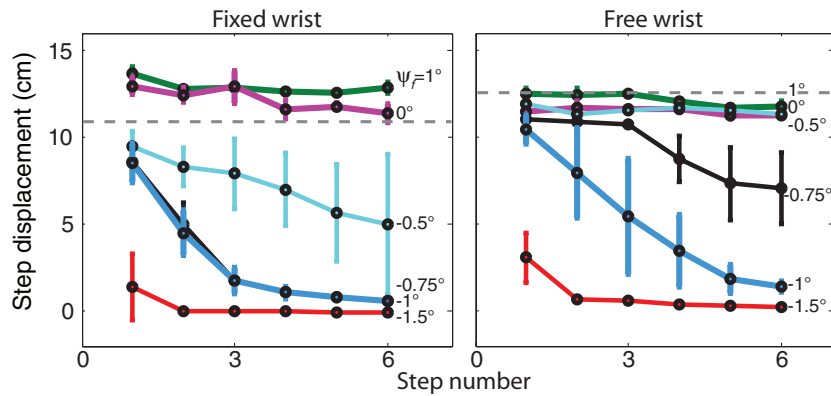


Figure 5. Step displacement, ΔS , depends sensitively on the flipper insertion depth, ψ_f , and wrist configuration. For sufficient flipper insertion, successive ΔS are equal and comparable in magnitude to model predictions in the absence of disturbed ground interaction (dashed horizontal lines), see section 4. For shallower insertion, successive ΔS decrease to zero indicating gait failure. $\theta_f = 90^\circ$ in both plots.



Figure 6. Tracks of FBot in poppy seeds for fixed and free wrist configurations with $\theta_f = 45^\circ$ and $\psi_f = 0$ (the black arrow indicates direction of robot motion). The vertical yellow line marks the location of initial flipper insertion, while left arrowheads mark visible extent of disturbed ground which, for the fixed wrist, is significantly larger and extends into the track from the previous step.

fixed wrists had a larger range of Δd over which the second step size was reduced, other parameters being equal.

The data in figure 7 indicate that when $\Delta S_1 < \Delta d_c$ gait failure can occur. To test this prediction we measured ΔS_n for the same conditions, see figure 8. When $\psi_f = 0$, $\Delta S > \Delta d_c$ for both wrist configurations and all θ_f , and the step size was constant as expected. Similarly, for the fixed wrist configuration with $\psi_f = -1^\circ$, failure occurred when $\Delta S_1 \lesssim \Delta d_c$. However, for the free wrist with $\psi_f = -1^\circ$,

failure occurred at $\theta_f \in \{67^\circ, 90^\circ\}$ even though $\Delta S_1 > \Delta d_c$; this behavior is discussed in section 4.

Gait failure occurs when flipper thrust forces are insufficient to overcome the drag force on the base of the locomotor, and, as shown above, is associated with a decreased separation between successive steps. To investigate this connection, we conducted experiments that measured the changes in the drag force, F_d , and penetration force, F_p , on a flat plate intruder for a two-step translation protocol similar to that described above for FBot. Using a vertical and horizontal translation stage, the plate was intruded 3 cm into the ground and then dragged backward 3 cm at a constant depth, creating a region of disturbed ground. The plate was withdrawn, moved forward to its initial position and then advanced a further distance Δd . Figure 9(A) shows F_p and F_d versus time for two distinct Δd during insertion and drag. F_p increased with the penetration depth approximately quadratically (tangential frictional forces on the sides are expected to dominate the normal force on the narrow bottom of the plate [17]), and the maximum value of F_p , which occurred at deepest penetration, increased with increasing Δd . When the plate was dragged horizontally, F_p fell to zero almost immediately, and F_d increased rapidly. For all but the smallest Δd , F_d reached a plateau after approximately 0.1 cm of horizontal motion, and for all Δd , F_d reached the plateau before the horizontal drag ended.

The maximum penetration force during vertical intrusion was reduced in the vicinity of the first depression (for $\Delta d < 3$ cm), see figure 9(B). This reduction was due to the decrease in the surface height surrounding the first intrusion which delayed the plate–ground contact (compare F_p for $\Delta d = 1$ cm and $\Delta d = 11$ cm in figure 9(A)). Consequently, maximum penetration was reduced since the intrusion depth (3 cm) was measured relative to the undisturbed surface. The mean drag force was reduced over a larger range of displacements, $\Delta d < 11$ cm, see figure 9(B). For Δd in this range, the ground displaced during the second horizontal motion encompassed the depression from the first intrusion. For $\Delta d < 6$ cm, as the horizontal motion began, the plate pushed the material into the depression and F_d was less than its mean value, while at the end of the motion the plate pushed the material up the rear

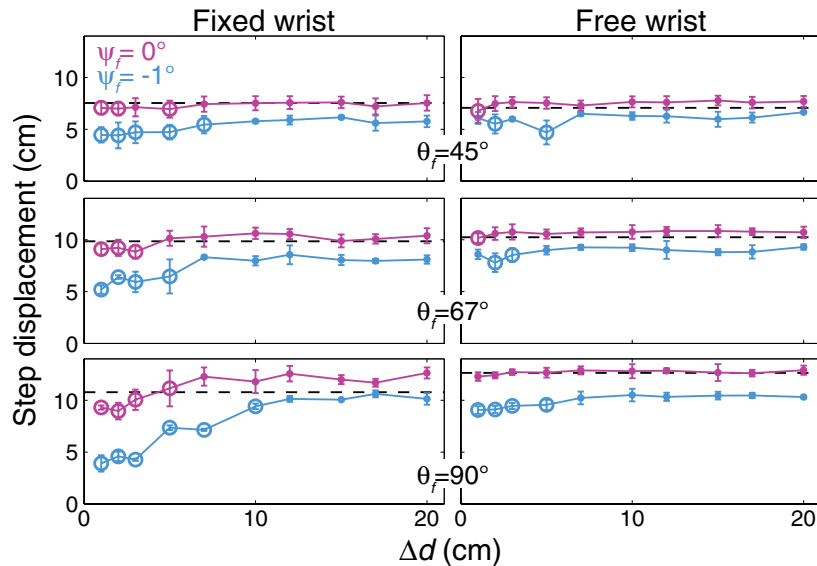


Figure 7. To study the influence of disturbed ground, FBot is placed Δd ahead of its position prior to its first step, and the average length of its second step, ΔS_2 , is plotted versus Δd for varying wrist configuration, θ_f and $\psi_f = 0$ (magenta) and $\psi_f = -1^\circ$ (blue). Open symbols denote where $\Delta S_2 < 0.95\Delta S_1$ and indicate where ground disturbed during the first step reduces the second step length. Horizontal dashed lines are predictions from free and fixed wrist models at each θ_f , see section 4.

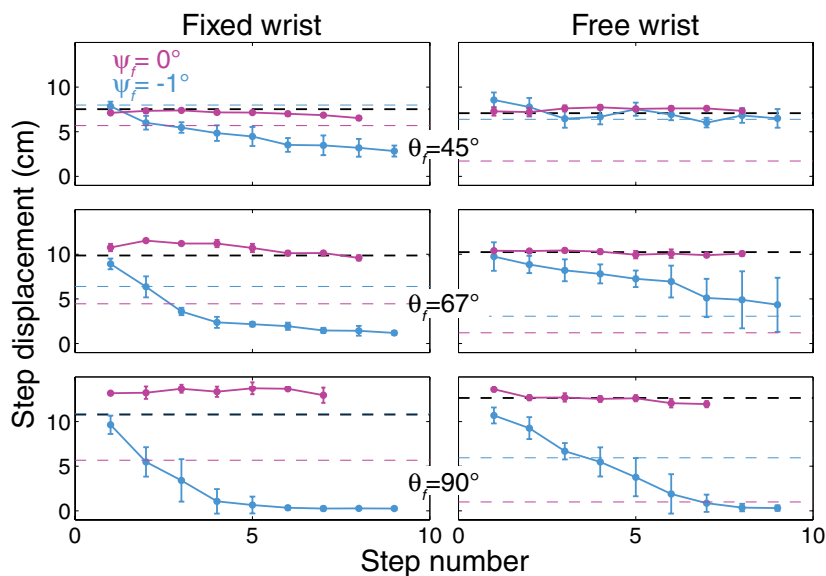


Figure 8. Average step displacement, ΔS , versus step number for varying wrist configuration, θ_f and ψ_f , together with Δd_c from figure 7 (colored horizontal dashed lines) below which disturbed ground reduces step displacement. For the fixed wrist (left), when $\Delta S_1 \lesssim \Delta d_c$, ΔS decreases monotonically with step number, leading to gait failure. For the free wrist (right), ΔS decreases with step number for $\psi_f = -1^\circ$ and $\theta_f \in \{67^\circ, 90^\circ\}$ even though $\Delta S_1 > \Delta d_c$ due to downward tilt when flippers move behind the COM. Black horizontal dashed lines are predictions from free and fixed wrist models, see section 4.

slope of the depression which increased F_d above its mean value. For $\Delta d > 12$ cm F_d was constant, indicating that the flipper was unaffected by ground disturbed in the first cycle.

To place the magnitudes of F_p and F_d in figure 9 in context with the forces required to lift and propel the robot, we measured the lift force, F_L , on FBot's flippers at $\theta = 0$ required to tilt it upward about the posterior axis and the drag force on its base, F_{db} , at $\alpha = 0$ and $\alpha = 4^\circ$. We found $F_L = 4.14 \pm 0.04$ N, $F_d(\alpha = 0) = 2.4 \pm 0.02$ N and $F_{db}(\alpha = 4^\circ) = 1.6 \pm 0.2$ N indicating that the measured flipper penetration and drag forces were sufficient to initially lift and advance FBot.

3.3. Hatchling sea turtle kinematics

To determine if the decreased performance associated with disturbed ground interaction observed for FBot also occurred in flippers biological locomotors, we analyzed videos (available from stacks.iop.org/BB/8/026007/mmedia) of hatchling loggerhead sea turtles running on level sand. The videos were taken in the field on Jekyll Island, GA in 2010 using the methods of our previous sea turtle hatchling research, see [17] for details. Each run (the turtles used a diagonal gait) was categorized as to whether or not visibly disturbed surface regions overlapped on successive steps, see figure 10,

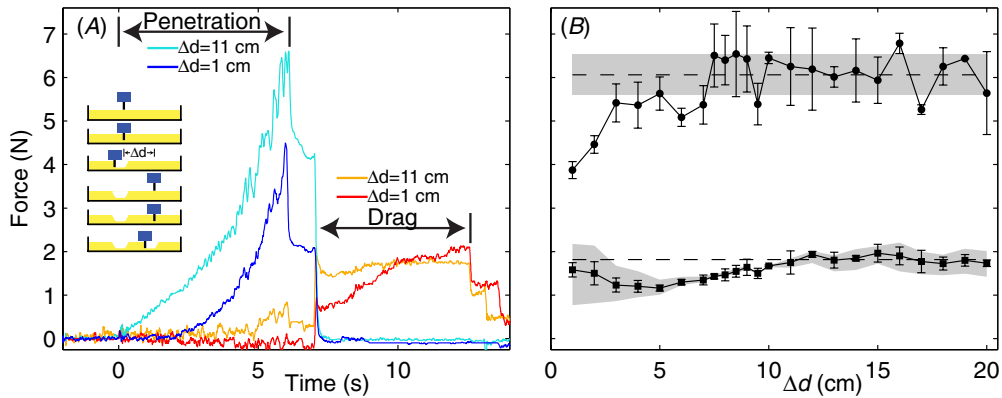


Figure 9. Forces on a 5 cm wide plate (similar in size to FBot’s flipper) during vertical penetration and horizontal drag at 0.5 cm s^{-1} depend on distance from disturbed ground Δd . (A) Penetration force, F_p , increases rapidly as the plate is moved downward ($0 < t < 6 \text{ s}$), while drag force, F_d , increases more gradually as the plate is moved horizontally ($7 \text{ s} < t < 13 \text{ s}$). Note that F_p drops almost immediately to 0 with the onset of horizontal drag. Inset: side-view depiction of sand (yellow) and drag apparatus (dark blue) illustrating penetration and drag protocol. (B) Peak penetration force (circles) decrease substantially only near the disturbed ground ($\Delta d < 3 \text{ cm}$), while the mean drag force (squares) is reduced over a larger distance ($\Delta d < 10 \text{ cm}$). Dashed lines show the mean values of F_p (upper) and F_d (lower) for $\Delta d > 10 \text{ cm}$, and the vertical bounds of the upper gray region indicate $\sigma(F_p)$ for the same range. Upper and lower vertical bounds of the lower gray region indicate the mean value of F_d for the first and last quarter of the drag interval, respectively.

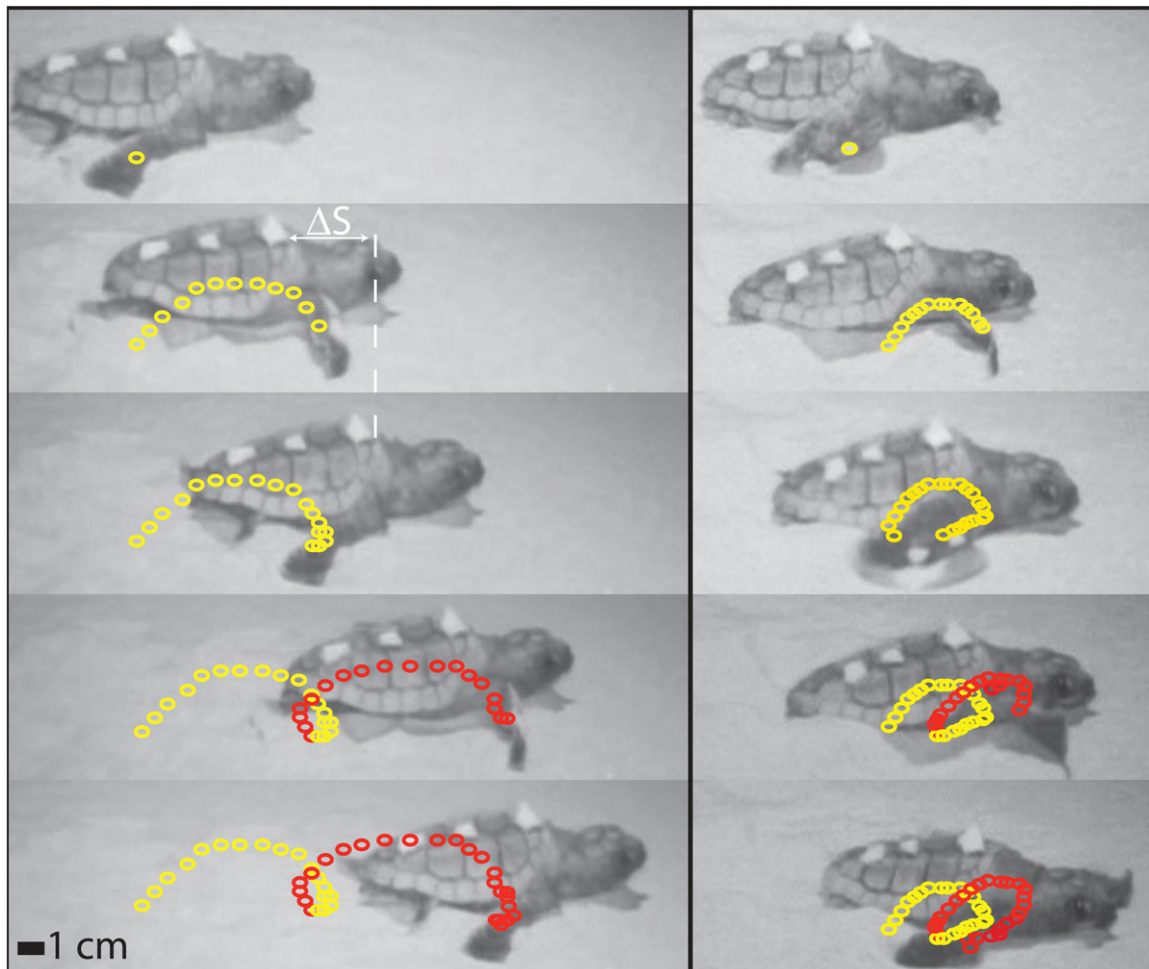


Figure 10. Two gait cycles of a loggerhead sea turtle hatchling, from two separate runs, with (left) no step overlap and (right) step overlap and tracked (circles) front right flipper wrist location. When per step displacement ΔS is small, the front flipper during the second step (red) interacts with ground disturbed on the previous step (yellow), see the lower-right panel. Trials were conducted in the field on a trackway of level, loose, beach sand. The turtles propelled themselves using a diagonal gait.

and the average speed and stride frequency were measured, (2–5 Hz), the average speed was higher for runs without overlap than for the runs with overlap ($P < 0.001$). In addition,

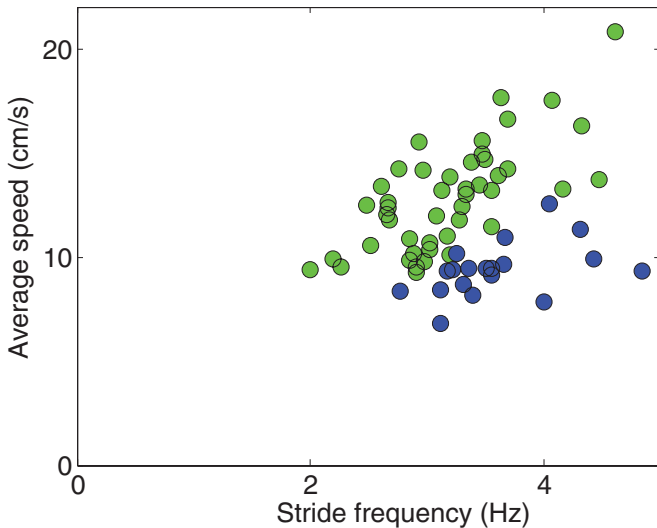


Figure 11. Average speed of loggerhead sea turtle hatchlings increases more rapidly with stride frequency when step interaction is small (green) than when successive steps interfere via disturbed ground (blue). Data collected in the field from $N = 66$ trials with $N = 25$ animals running on a trackway of level, loose sand.

the slope of the speed–frequency relationship was significantly higher ($P < 0.001$) for runs without overlap than for the runs with overlap.

4. Discussion

We now discuss how the interaction of limb intrusion, belly friction, disturbed ground and wrist configuration determine locomotor effectiveness, and we develop quantitative models that accurately predict the observed behavior. FBot’s motion depended sensitively on limb kinematics, and the free wrist was more robust than the fixed. To understand these behaviors, we start by recognizing that locomotion is wholly determined by thrust and drag forces. For a prescribed limb motion, thrust increased with greater flipper penetration or greater flipper distance from previously disturbed ground. Thrust depends sensitively on the penetration depth because both the area of the flipper in ground contact and the yield strength of the substrate increase approximately linearly with the depth, which leads to an overall depth-squared dependence of the thrust [17]. In contrast, drag is reduced by raising the anterior so that it does not plow into the substrate, or, if there is no upward tilt ($\alpha = 0$), increasing the vertical force on the flippers through deeper penetration, which reduces the normal force on the base and thus the frictional drag on the base. To better understand the origin and influence of thrust and drag, we describe in greater detail the dynamics of FBot’s gait and model its motion for the free and fixed wrist configurations when per step displacement, ΔS , is sufficiently large that steps do not interfere. We then use the models to better understand why locomotion depends sensitively on the flipper insertion depth and how disturbed ground-induced decreases in penetration and thrust forces contribute to locomotion failure.

We focus first on flipper penetration. As the flippers are rotated downward into the substrate, the vertical substrate

penetration force, F_p , increases with the flipper penetration depth, z , to oppose the motion and generates an equal and opposite lift force, $F_L = -F_p$, on the flippers. For sufficient flipper penetration depth, the torque about the posterior base contact line from the lift force, τ_L , exceeds the opposing gravitational torque, τ_g , acting at the COM. This causes FBot to tilt upward about the posterior axis (assuming the flippers are in front of the COM). Once upward tilt begins, the flipper depth remains constant as the gravitational torque decreases with increasing α , i.e. $\tau_g = mgl_{\text{com}} \cos \alpha$, where l_{com} is the distance from the posterior line to the COM and g is the acceleration due to gravity. If τ_L is less than τ_g , no upward rotation occurs ($\alpha = 0$), and the flipper penetration depth is determined solely by ψ_f .

To quantify body tilt, we balance the gravitational torque and flipper generated lift torque about the posterior axis:

$$F_L l_w \cos \alpha - mgl_{\text{com}} \cos \alpha = 0,$$

where l_w is the fore–aft distance from the posterior to the wrist axis. The lift force required to raise the front of FBot is then

$$F_L = mg \frac{l_{\text{com}}}{l_w}. \quad (1)$$

As the flippers rotate toward the rear with increasing θ , l_w decreases which increases F_L . For $\alpha > 0$, equation (1) indicates that the vertical lift force on the flippers increases to a maximum of mg at $l_w(\theta) = l_{\text{com}}$ which occurs at $\theta \approx 50^\circ$ for FBot (see figure 2). The increase in F_L drives the flippers deeper into the substrate. If the robot is tilted upward when the flippers pass behind the COM, then it tips downward and drives its leading edge into the substrate, which greatly increases the drag force and creates a pile of material at the front.

Since F_L and l_w are known functions of θ , the flipper penetration depth, z , and thus the tilt angle can be predicted when $F_p(z)$ is known. We obtained $F_p(z)$ (see inset of figure 12(A)) for FBot’s flippers by averaging seventy penetration force profiles of the first insertion, which occurs in undisturbed ground, from the penetration and drag experiments (figure 9) and scaling the average by $2 \times 7/5$, where the first number accounts for FBot’s two flippers and the second is the ratio of FBot’s flipper width to the plate width in the penetration and drag force experiments. Figure 12(A) shows that for $\theta < 50^\circ$ the predicted value of α is nearly constant, which is qualitatively similar to the measured value for the free wrist, but is different from the measured value for the fixed wrist⁷ which decreases continuously with increasing θ . For the free wrist, predicted α is larger by $\approx 1^\circ$ for $\theta < 50^\circ$ compared to experiment⁸.

For $\theta > 50^\circ$, however, the model predicts an average downward tilt of $\alpha \approx -3^\circ$ while we measure $\alpha \approx 0$ for both free and fixed wrist experiments. We hypothesize that this discrepancy occurs because the model ignores increases in drag associated with the downward tilting posture and the

⁷ Measured values of α for free and fixed wrists are equal at $\theta = 0$ where the wrist configuration has no influence.

⁸ Better agreement with the free wrist data for $\theta < 50^\circ$ is achieved by accounting for the finite holding torque of the up–down servo motors (61 N cm deg^{-1}) which reduces the commanded insertion angle as F_L increases.

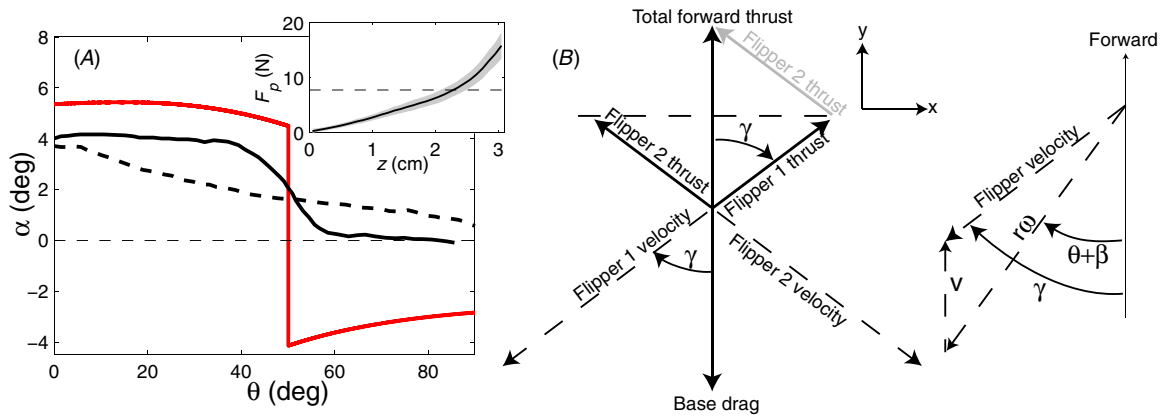


Figure 12. Modeling FBot tilt and step displacement. (A) FBot tilt versus limb angle for free (black) and fixed (dashed black) wrist experiments compared to predictions using penetration force (red) for $\theta_f = 90^\circ$ and $\psi_f = 0$. Downward tilt (raised posterior, $\alpha < 0$) predicted by the model when COM is in front of flippers for $\theta > 50^\circ$ is not observed in experiment, although, for the free wrist, $\theta \approx 50^\circ$ marks the middle of the region of rapid decrease in α for all θ_f (see text for discussion). Inset: average penetration force versus depth, z , from insertion experiments; shaded region is $\pm\sigma$. Horizontal line indicates the FBot weight. (B) COM force balance model for FBot locomotion with fixed wrist illustrating how (left) fore–aft force balance with simultaneous slip of flippers and base sets slip angle γ which in turn (right) determines robot velocity v in the lab frame (see text). Solid (dashed) vector denotes forces (velocities).

possible influence of disturbed ground in front of FBot. For example, a pile of material plowed up in front of FBot (see row 4 of figure 3) would limit flipper sinkage during subsequent steps and could potentially eliminate most downward tilt if the pile were in front of the COM when the flippers passed behind the COM. Step displacement data from figure 8 for the free wrist supports this hypothesis as failure occurs even when $\Delta S_1 > \Delta d_c$ at $\psi_f = -1^\circ$ for $\theta_f \in \{67^\circ, 90^\circ\}$ but no failure occurs for the same conditions with $\theta_f = 45^\circ$ where the flippers remain in front of the COM and downward tilt is absent.

We next consider FBot’s per step displacement. As shown in figure 6, the fixed and free wrist motions of FBot’s flippers through the substrate differ substantially. For the fixed wrist configuration, FBot’s flippers are constrained to rotate with the limb so that the flippers always locally yield (fluidize) the ground as evidenced by the large disturbed ground region. As discussed above (see figure 9), when the flipper slips backward after penetration the lift force rapidly decreases. This effect is consistent with the constant decrease in tilt shown in figures 4 and 12 for the fixed wrist and has been observed in other geometries when granular materials are sheared [18]. For the free wrist, the wrist axis again rotates about the fore–aft motor axis, but in this configuration the flipper maintains its initial orientation orthogonal to the medial line of FBot. The result is that during the step the flipper slides away and then toward the body but does not move backward through the ground, as figure 6 shows. The tilt data shown in figures 4 and 12 are again consistent with this picture, as backward slippage of the free wrist flippers when in front of the COM would cause a more rapid decrease in α with increasing θ than is observed.

Based on these differences in ground interaction, we construct a model of FBot’s successful motion for each wrist configuration. For the free wrist, FBot’s motion is determined by the limb kinematics with the assumption that the flipper does not slip backward relative to the ground but can slip laterally. With these assumptions, the instantaneous forward velocity during the step, $v(t)$, and the step size are

$$v(t) = r\omega \cos(\omega t + \beta) \quad (2)$$

and

$$\Delta S = r[\sin(\theta_f + \beta) - \sin \beta], \quad (3)$$

where t is the time, r is the length of the line segment connecting the fore–aft motor axis to the wrist axis, and $\beta = -28^\circ$ measures the angle of this line relative to a lateral line when θ is zero⁹. Predictions from equation (2) for $\theta_f = 45^\circ$ and $\theta_f = 90^\circ$ are shown in rows 1 and 2, respectively, of the last column of figure 3. The predicted velocities agree well with the measured values except for a spike in the experimental data near $\theta = 45^\circ$. This θ value is close to where the tilt model predicts FBot should pitch forward when its COM moves in front of its flippers and is similar to the negative peak in the velocity that occurs at the beginning of the stance phase when the tracking markers move upward and back with increasing α . Predicted values of ΔS for equation (3) are shown in figures 5 and 8 and are in good agreement with measured free wrist values when flippers do not slip backward.

To model forward motion with the fixed wrist, we assume that per flipper thrust force, \vec{F}_{if} , is opposite to the flipper’s instantaneous velocity relative to the stationary substrate (lab frame) at an angle γ measured from the forward direction, see figure 12(B). In the figure, solid (dashed) vectors denote forces (velocities). When the magnitude of the total forward thrust from both flippers $F_t = 2F_{if} \cos \gamma$ equals the drag from the belly of the robot, F_{db} , the robot advances. Since both the robot base and flippers slip simultaneously relative to the ground during the forward motion, the components of force in the forward direction sum to zero when acceleration is neglected. The zero net force condition then requires

$$\tan \gamma = \sqrt{\left(\frac{2F_{if}}{F_{db}}\right)^2 - 1}.$$

In the body frame of the robot the flipper velocity is $\vec{v}_B = -r\omega(\sin \phi, \cos \phi)$, where $\phi = \theta + \beta$, which in the lab frame

⁹ If FBot’s limb were straight and connected directly between the wrist axis and the fore–aft motor axis, β would be zero.

becomes $\vec{v}_L = (-r\omega \sin \phi, v - r\omega \cos \phi)$, where v is the forward velocity of FBot. Requiring that the flipper velocity and thrust force be opposite (i.e. $\tan \gamma = \frac{-r\omega \sin \phi}{v - r\omega \cos \phi}$) then determines the velocity as

$$v = r\omega \left[\cos(\omega t + \beta) - \frac{\sin(\omega t + \beta)}{\sqrt{\left(\frac{2F_{\text{tf}}}{F_{\text{db}}}\right)^2 - 1}} \right], \quad (4)$$

with the constraint that $\omega t + \beta < \gamma$, which is equivalent to requiring that the flippers always slip backward and the robot move forward. Velocity predictions from equation (4) for $\theta_f = 90^\circ$ are shown in rows 3 and 4 of figure 3 using measured constant values of $F_{\text{db}} = 2.4$ N and $F_{\text{tf}} = 2.6$ N which correspond to a 3 cm flipper penetration depth. The predicted velocities agree well with the measured values for the constant per step displacement gait. They agree with the data for the failure gait only at the beginning and end of the stroke where the flippers are outside the depressions dug by previous steps.

If F_{tf} and F_{db} are approximated as constant during the step, equation (4) can be integrated to give the step distance

$$\Delta S = r \left[\sin \phi_+ - \sin \phi_- + \frac{\cos \phi_+ - \cos \phi_-}{\sqrt{\left(\frac{2F_{\text{tf}}}{F_{\text{db}}}\right)^2 - 1}} \right], \quad (5)$$

where ϕ_+ is the smaller of γ or $\theta_f + \beta$ and ϕ_- is the larger of $-\gamma$ or β . Equation (5) matches the free wrist (equation (3)) in the limit that $F_{\text{tf}} \gg F_{\text{db}}$. Predicted values of ΔS from equation (5) for $F_{\text{db}} = 2.4$ N and $F_{\text{tf}} = 2.6$ N are shown in figures 5, 7 and 8 and are in good agreement with measured fixed wrist ΔS values when disturbed ground is not encountered and the insertion depth is sufficient (i.e. $2F_{\text{tf}} > F_{\text{db}}$), with the exception of the fixed wrist geometry with $\theta_f = 90^\circ$. In this case, measured ΔS is larger than predicted: we hypothesize that the substrate material pushed up behind the slipping flippers and squeezed against the body increases flipper thrust without significantly increasing base drag.

When disturbed ground is encountered, equations (1)–(5) provide insight into how gait failure occurs. Tilt decreases at initial flipper insertion and decreases more rapidly during the stride due to the reduction in the penetration force. The decrease in tilt brings the body into contact with the ground sooner and for larger ψ_f and, consequently, the average drag force per step increases. If tilt is sufficient to keep $\alpha > 0$ during the step stage, then locomotion for the free wrist should remain largely unaltered as the thrust force increases and drag force decreases during the step as weight is transferred to the flippers, increasing penetration and reducing base friction. In contrast, FBot with a fixed wrist ceases to advance when thrust becomes less than drag. Since the flippers slip backward, they move closer to the ground disturbed during the previous step. If the weakened ground is encountered, forward motion will be reduced, which can initiate failure. Successive failed strokes dig a relatively deep hole which eventually leaves the robot unable to generate sufficient lift and thrust forces to move at all.

FBot's failure modes offer insight into how sea turtles potentially mitigate locomotory failure. Downward tilt with ground contact and subsequent pile formation can be avoided by keeping the COM behind the leading flipper through the control of the gait amplitude or by advancing the opposite flipper ahead of the COM for alternating gaits. Alternatively, turtles can lower their bodies to the ground before the COM passes in front of the lead flipper(s) to avoid the downward tilt. If flipper slip occurs, turtles can raise their plastron off the ground using both front and hind limbs to eliminate drag forces or increase the flipper penetration depth to increase thrust. Turtles can also vary the pitch of their flippers [17] which provides a control of penetration depth for the same downward flipper force. Although figures 10 and 11 indicate that hatchling sea turtle locomotor performance is greater when step interaction via the disturbed ground is minimized, the question of which, if any, of the potential methods described above the turtles use remains open. Additionally, and unlike our robot experiments, turtles sometimes traverse sandy slopes which alters the physics of force balance and substrate load bearing capacity, and potentially leads to different kinematics and control strategies for both animals and robots. We are currently investigating this topic.

5. Conclusion

Previous research on hatchling loggerhead sea turtles revealed varying flipper use dependent on beach substrate properties [17]. Motivated by this work, we developed and tested a sea turtle-inspired physical model, FBot, to better understand the principles of flipper-based locomotion on granular media. We tested FBot with two wrist configurations and various gaits and found that the sea turtle-inspired free wrist generated larger per step displacement for a range of parameters. The added degree of freedom of the free wrist joint allowed the robot to maintain flipper applied stress below the substrate yield stress and advanced its body kinematically with no slip. In contrast, the fixed wrist constantly yielded the substrate as the flippers propelled the body forward and consequently increased body drag during stance. These two modes of propulsion resulted in differing step profiles as well as limb-ground interactions. Further, we found that FBot was sensitive to the flipper insertion depth—a small decrease in flipper penetration could greatly reduce the step displacement, which was cumulative as the step number increased and ultimately resulted in no movement of the body. Key findings were that when flippers interacted with the ground disturbed during previous steps or the robot tilted downward, performance was reduced. Models of tilt and forward motion showed quantitative agreement with the experimental data and revealed the importance of body tilt and thrust direction during flipper slip. Further biological and physics studies are required to determine how substrate compaction as well as the incline angle affects the performance of animals and physical models that locomote on granular media.

The interacting effects of body lift, flipper thrust, base drag, ground yielding and disturbed ground for FBot indicate that effective flippered locomotion on granular media is not

trivial. To advance, an animal or robot must insert its flippers sufficiently deep to both reduce drag on its base/belly via flipper lift and generate sufficient thrust to overcome body drag. A large step distance allows the body to move past the zone of ground disturbed on the previous step so that sequential steps are unaffected by deformable material. If the limb is inflexible, rotation in the sand will increase penetration. If the limbs are fully extended beneath the belly, loss of upward tilt can lead to failure as slipping flippers produce little, if any, lift forces which increase drag by increasing the normal force on the base/belly. Even with sufficient lift and minimal slippage, failure can still occur if the COM advances beyond the leading limb(s). When this occurs, the front pitches downward and plows into the substrate, which generates larger drag forces and a pile that impedes motion.

Robot modeling allows tests of locomotion hypotheses involving gait and morphology that are currently beyond the capacity of animal experimentation and can potentially shed light on possible origins of successful animal structures and controls. For example, animals, like lobe-finned fishes, likely first walked on wet sand and mud [2, 27, 31]. In the evolutionary transitions from aquatic to terrestrial locomotion, the rheology of limb (fin/flipper) interaction changed from slipping through fluid to pushing against materials that can be fluid or solid. Locomotor strategies thus changed as bodies and appendages shifted from generating thrust during swimming to generating both lift (to maintain posture and reduce ground contact) and thrust (to propel the body). However, as little is known of the biomechanics of walking/crawling on soft substrates, detailed hypotheses are lacking for how limbs and control strategies adapted to these substrates. Combined with detailed anatomical studies of the morphology and range of motion of appendages of fossils [19], robot-based studies will allow better modeling of early terrestrial locomotors.

Finally, bio-inspired robotics investigations can help identify common principles of biological design and realize those principles in physical devices [12]. AmphiBot, SnakeBot and RHex [10, 4, 25, 12] are examples of bio-inspired robots used to study locomotor patterns during swimming, crawling or walking [20]. RHex was inspired by research on arthropod runners with the intent of uncovering the control architecture that enables effective locomotion in complex terrestrial environments [12]. FBot is among the first robots to employ flippers instead of legs, wheels or other appendages to interact with yielding terrestrial substrates and, as such, could be a model for future multi-terrain robots able to swim and run effectively using the same appendages for both media [33]. Additionally, using granular media, for which mechanical properties can be precisely controlled over a range of values (see e.g. [8]), as a model yielding substrates can give insight into locomotion on other more complex materials such as mud, wet sand, leaf litter and snow.

Acknowledgments

We thank Nick Gravish, Matthew Jacobson and Azeem Bandede-Ali for sharing their tracking, servomotor control

and force measurement code, respectively, and Andrei Savu, Lauren Townsend, Helena Mazouch and the Georgia Sea Turtle Center for assistance in the field. Work supported by the Burroughs Wellcome Fund Career Award at the Scientific Interface, NSF CMMI-0825480, NSF PoLS number PHY-1150760, ARO Grant No. W911NF-11-1-0514 and ARL MAST CTA under cooperative agreement number W911NF-08-2-0004.

References

- [1] Alexander R M 2003 *Principles of Animal Locomotion* (Princeton, NJ: Princeton University Press)
- [2] Clack J A 2002 *Gaining Ground: The Origin and Early Evolution of Tetrapods* (Bloomington, IN: Indiana University Press)
- [3] Clark J E and Cutkosky M R 2006 The effect of leg specialization in a biomimetic hexapedal running robot *Trans. ASME, J. Dyn. Syst. Meas. Control* **128** 26
- [4] Crespi A, Badertscher A, Guignard A and Ijspeert A J 2005 Swimming and crawling with an amphibious snake robot *ICRA'05: Proc. IEEE Int. Conf. on Robotics and Automation* pp 3024–8
- [5] Delcomyn F 2007 Biologically inspired robots *Bioinspiration and Robotics: Walking and Climbing Robots* (Vienna: I-Tech) pp 279–300
- [6] Dickinson M H, Farley C T, Full R J, Koehl M A R, Kram R and Lehman S 2000 How animals move: an integrative view *Science* **288** 100–6
- [7] Fish F E, Hurley J and Costa D P 2003 Maneuverability by the sea lion *Zalophus californianus*: turning performance of an unstable body design *J. Exp. Biol.* **206** 667
- [8] Gravish N, Umbanhowar P B and Goldman D I 2010 Force and flow transition in plowed granular media *Phys. Rev. Lett.* **105** 128301
- [9] Gulko D and Eckert K L 2004 *Sea Turtles: An Ecological Guide* (Honolulu, HI: Mutual Publishing)
- [10] Ijspeert A, Crespi A, Ryczko D and Cabelguen J M 2007 From swimming to walking with a salamander orbit driven by a spinal cord model *Science* **315** 1416–20
- [11] Jaeger H M, Nagel S R and Behringer R P 1996 Granular solids, liquids and gases *Rev. Mod. Phys.* **68** 1259–73
- [12] Koditschek D E, Full R J and Buehler M 2004 Mechanical aspects of legged locomotion control *Arthropod Struct. Dev.* **33** 251–72
- [13] Li C, Hsieh S T and Goldman D I 2012 Multi-functional foot use during running of the zebra-tailed lizard (*Callisaurus draconoides*) *J. Exp. Biol.* **215** 3293
- [14] Li C, Umbanhowar P B, Komsuoglu H and Goldman D I 2010 The effect of limb kinematics on the speed of a legged robot on granular media *Exp. Mech.* **50** 1383–93
- [15] Li C, Umbanhowar P B, Komsuoglu H, Koditschek D E and Goldman D I 2009 Sensitive dependence of the motion of a legged robot on granular media *Proc. Natl Acad. Sci.* **106** 3029
- [16] Li C, Zhang T and Goldman D I 2013 A terradynamics of locomotion on flowing ground *Science* **339** 1408
- [17] Mazouchova N, Gravish N, Savu A and Goldman D I 2010 Utilization of granular solidification during terrestrial locomotion of hatchling sea turtles *Biol. Lett.* **6** 398–401
- [18] Nichol K and van Hecke M 2012 Flow-induced agitations create a granular fluid: effective viscosity and fluctuations *Phys. Rev. E* **85** 061309
- [19] Pierce S E, Clack J A and Hutchinson J R 2012 Three-dimensional limb joint mobility in the early tetrapod *Ichthyostega* *Nature* **486** 523–6

- [20] Saranli U, Buehler M and Koditschek D E 2001 Rhex: a simple and highly mobile hexapod robot *Int. J. Robot. Res.* **20** 616–31
- [21] Albert I, Tegzes P, Albert R, Sample J G, Barabási A-L, Vicsek T, Kahng B and Schiffer P 2001 Stick-slip fluctuations in granular drag *Phys. Rev. E* **64** 031307
- [22] Swanson B O and Gibb A C 2004 Kinematics of aquatic and terrestrial escape responses in mudskippers *J. Exp. Biol.* **207** 4037
- [23] Vogel S 1996 *Life in Moving Fluids: the Physical Biology of Flow* (Princeton, NJ: Princeton University Press)
- [24] Wiegardt K 1975 Experiments in granular flow *Annu. Rev. Fluid Mech.* **7** 89–114
- [25] Wright C, Johnson A, Peck A, McCord Z, Naaktgeboren A, Gianfortoni P, Gonzalez-Rivero M, Hatton R and Choset H 2007 Design of a modular snake robot *IROS'2007: IEEE/RSJ Int. Conf. on Intelligent Robots and Systems* pp 2609–14
- [26] Wyneken J 1997 Sea turtle locomotion: mechanisms, behavior and energetics *Biol. Sea Turtles* **1** 165–98
- [27] Zimmer C 1999 *At The Water's edge: Fish with Fingers, Whales with Legs and How Life Came Ashore but then Went Back to Sea* (New York: Free Press)
- [28] Maladen R D, Ding Y, Umbanhowar P B, Kamor A and Goldman D I 2011 Mechanical models of sandfish locomotion reveal principles of high performance subsurface sand-swimming *J. R. Soc. Interface* **8** 1332–45
- [29] Shubin N 2009 *Journey into the 3.5 Billion Year History of the Human Body* (New York: Knopf Doubleday)
- [30] Steyer S 2012 *Earth before the Dinosaurs* (Indiana University Press)
- [31] Shubin N H, Daeschler E B and Jenkins F A 2006 The pectoral fin of *Tiktaalik roseae* and the origin of the tetrapod limb *Nature* **440** 764–71
- [32] Ding Y, Sharpe S S, Masse A and Goldman D I 2012 Mechanics of undulatory swimming in a frictional fluid *PLoS Comput. Biol.* **8** (12) e1002810
- [33] Xu M, Xu L, Liu P, Ren X, Kong Z, Yang J and Zhang S 2012 The AmphiHex: a novel amphibious robot with transformable leg-flipper composite propulsion mechanism *IROS 2012: IEEE/RSJ Int. Conf. on Intelligent Robots and Systems* pp 3667–72